nature communications

Article

https://doi.org/10.1038/s41467-025-62082-5

Identification of a key nucleotide influencing Cas12a crRNA activity for universal photo-controlled CRISPR diagnostics

Received: 9 March 2025

Accepted: 10 July 2025

Published online: 21 July 2025

Check for updates

Tian Tian[1,4] ✉, Hongrui Xiao[1,4], Xinyi Guo[1], Yuxin Chen[1], Zhiqiang Qiu[1], Ting Zhang[1], Meiyu Chen[1], Weiwei Qi[1], Peige Cai[1], Meng Cheng[2] & Xiaoming Zhou[1,3] ✉

Developing a one-pot assay is a critical strategy for enhancing the applicability of CRISPR-based molecular diagnostics; however, it is hindered by CRISPR cleavage interfering with nucleic acid amplification templates. Photo-regulation strategies provide an ideal solution to suppress undesired CRISPR cleavage while maintaining detection efficiency. However, existing photo-controlled CRISPR diagnostic methods face limitations in universality, cost, and detection efficiency. In this study, we systematically examine the impact of mutations in the repeat recognition sequence (RRS), a four-nucleotide segment within the Cas12a crRNA direct repeat (DR) region, on cleavage activity. We observe that mutations at positions 3 or 4 nearly abolished crRNA activity. Based on this discovery, we introduce 6-nitropiperonyloxymethyl (NPOM) photo-caging modifications at positions 3 and 4. Photo-caging at position 4 demonstrates the most effective suppression of enzymatic activity and optimal light-mediated activation. We leverage this finding to develop a photo-controlled CRISPR diagnostic method, enabling a universally adaptable one-pot detection strategy. Furthermore, by incorporating a crRNA splinting strategy, this pre-preparable reagent can be adapted for the detection of virtually any target gene.

CRISPR is an adaptive immune system initially discovered in prokaryotes, which was later reconstructed in vitro and repurposed for genome editing[1–3]. Approximately nine years ago, it was first applied to nucleic acid detection[4], leading to the rapid evolution of various CRISPR-based molecular diagnostic techniques[5–7]. Among these CRISPR detection systems, Cas13a and Cas12a are the most widely adopted due to their advantages in detection efficiency and component simplicity. These two systems have been previously demonstrated to specifically recognize RNA and DNA, respectively, and activate their *trans*-cleavage activities[8–11]. Recent studies have further revealed that both Cas13a and Cas12a possess the capability to recognize both DNA and RNA[12–17]. Compared to Cas13a, the Cas12a system appears to be more advantageous for diagnostic applications, as it exhibits a comparable cleavage efficiency to Cas13a but requires a shorter crRNA (~40 bp).

CRISPR diagnostic technology has garnered much praise due to its homogeneous detection mode based on *trans*-cleavage activity, sequence-specific enzyme activation mechanism, and mild reaction conditions. It is expected to drive the development of next-generation diagnostic technologies. However, several key technical challenges

[1]School of Life sciences, South China Normal University, Guangzhou, China. [2]Department of Clinical Laboratory, The First Affiliated Hospital of Guangzhou Medical University, Guangzhou, China. [3]MOE Key laboratory of Laser Life Science & Guangdong Provincial Key Laboratory of Laser Life Science, College of Biophotonics, South China Normal University, Guangzhou, China. [4]These authors contributed equally: Tian Tian, Hongrui Xiao.
✉e-mail: ttian@m.scnu.edu.cn; zhouxm@scnu.edu.cn

must be addressed before they can be widely applied in clinical settings. For instance, despite their exceptional analytical sensitivity (with detection limits in the picomolar to femtomolar range), CRISPR-based assays still require pre-amplification of target nucleic acids to achieve clinically relevant detection, typically in the attomolar range. However, in early CRISPR-based detection technologies, nucleic acid amplification and CRISPR detection were typically performed as separate steps to prevent CRISPR-mediated cleavage from degrading the amplification template[18–20]. But this stepwise approach increased workflow complexity and introduced the risk of aerosol contamination from amplified products. A similar challenge arose in the early development of PCR, where open-tube electrophoresis was initially required for result analysis. The breakthrough that enabled PCR's widespread adoption was the development of closed-tube real-time quantitative PCR[21]. Likewise, integrating CRISPR cleavage with nucleic acid amplification into a one-pot reaction is essential for advancing CRISPR-based molecular diagnostics toward practical applications[22].

To address this challenge, some strategies physically separate nucleic acid amplification and Cas12a cleavage within a closed system, while others utilize microfluidic chips with spatially compartmentalized reactions[23–26]. However, these approaches often require manual post-reaction merging or custom-designed microfluidic chips, which can compromise reproducibility and limit usability in point-of-care testing (POCT) applications. It has been shown that adding high-viscosity additives to a one-pot detection system can delay the fusion of the reaction components, thereby reducing premature CRISPR cleavage[27,28]. However, these strategies are prone to operational errors, which can affect the reproducibility of results, and the reagents cannot be lyophilized. Recently, significant efforts have focused on developing methods to regulate CRISPR system activity. Early approaches included optimizing the one-pot reaction buffer to reduce Cas enzyme cleavage activity while minimizing the impact on nucleic acid amplification[23,29]. Another strategy involves weakening Cas12a's cleavage activity by using suboptimal PAM sites[30], reducing the enzyme's substrate affinity through molecular engineering[31], or adding inhibitors, such as heparin[32], to suppress Cas12a activity, enabling one-pot CRISPR-Cas12a detection. However, these methods only alleviate, rather than completely eliminate, competitive cleavage of nucleic acid substrates, which may still limit the efficiency of the one-pot assay. Additionally, the weakened Cas12a system also affects the final detection efficiency.

Photo-controlled CRISPR method has been employed for spatiotemporal gene editing and has proven effective in reducing off-target effects[33–36]. Recently, we and other groups have developed photo-controlled methods to enable robust one-pot CRISPR detection[37,38]. This technique relies on designing oligonucleotides that can be photolyzed to block the spacer region of crRNA. Further improvements include embedding 6-nitropiperonyloxymethyl caged thymidine (NPOM-dT) in the spacer region to prevent hydrogen bonding between crRNA and target DNA, thereby shielding the recognition activity[39]. While these optimizations have significantly improved detection performance over conventional methods, challenges related to generalizability remain. For instance, changing the detection target requires re-screening of NPOM modification sites and the number of modifications. One potential solution is to use photo-cloaking agents to acylate all bases of crRNA, which addresses the generalizability issue[40]. However, such multi-base modifications are cumbersome, costly, and the complete recovery of activity remains challenging.

In this study, we aim to develop a more cost-effective and versatile photo-controlled CRISPR-Cas12a system. Our approach focuses on regulating the direct repeat (DR) region of crRNA, in contrast to the spacer region previously targeted. Previous research has demonstrated that the Cas12a system exhibits both DNase and RNase activities[9,10,41]. The DNase activity is responsible for *cis*- and *trans*-cleavage, while the RNase activity processes pre-crRNA into mature crRNA[42]. Evidence shows that Cas12a cleaves pre-crRNA at four nucleotides upstream of the stem-loop structure, suggesting that the residues between this region and the cleavage site are critical for substrate processing. This four-nucleotide sequence, known as the repeat recognition sequence (RRS), is part of the crRNA's DR region. Structural analyses have revealed that the RRS, once folded, interacts with the stem-loop to form a specific pseudoknot structure, which is essential for binding to Cas12a[43,44].

Previous studies have shown that mutations in the RRS region affect the Cas12a-mediated processing of precursor crRNA[42]. In this study, we hypothesize that mutations in these four nucleotides may also influence the *cis*- and *trans*-cleavage activity of the Cas12a system. Our screening experiments reveal that mutations in the third and fourth positions of the RRS led to nearly complete loss of crRNA functionality. Based on these findings, we replace these two positions with NPOM-dT, evaluate their photo-switching effects, and identify the U base at position RRS-4 as the optimal photo-responsive switch base. As a result, we develop a universal Photo-controlled CRISPR diagnostic technology that requires only a single-base modification in the crRNA. Furthermore, by adopting a split crRNA design, this split photo-caged crRNA reagent can be pre-prepared and applied to the detection of virtually any target.

Results

Identification of key nucleotides in the DR region of crRNA that influence Cas12a cleavage activity

Precise temporal regulation of the CRISPR-Cas system using light provides a powerful tool for accurate genetic manipulation and contributes to the development of highly sensitive, enhanced one-pot detection methods. However, existing photo-controlled strategies[37–40] face limitations in terms of generalizability, cost, and ease of design (Fig. 1a). Therefore, there is a pressing need to explore a low-cost, versatile, and easily designed crRNA regulatory strategy. Cas12a possesses intrinsic endonuclease activity, enabling direct cleavage of pre-crRNA located upstream of the crRNA pseudoknot. The first four nucleotides at the 5′ end of crRNA can form a pseudoknot structure by intramolecular pairing and hydrogen bonding with the stem-loop structure of the DR region. These four nucleotides are referred to as the RRS, which plays a crucial role in the processing of pre-crRNA (Fig. 1b). Previous work has demonstrated that single-base mutations in the RRS significantly affect Cas12a's cleavage activity on pre-crRNA processing[42].

Based on this, we propose that studying the critical region of crRNA could help identify the key nucleotides for LbCas12a's *cis*- and *trans*-cleavage activities. To investigate how mutations at different positions within the RRS affect crRNA's *trans*-cleavage activity, we introduced single-base mutations at positions 1–4 of the RRS in eight crRNAs (mutating A to U/G/C at positions 1 and 2, and U to A/G/C at positions 3 and 4) (Fig. 1c). Fluorescence assays revealed significant differences in *trans*-cleavage activity among the various crRNA variants (Fig. 1d and Supplementary Fig. 1). Compared to the wild-type, mutations at any position in the RRS significantly impacted *trans*-cleavage activity, with the following order of effect: position $4 \approx 3 > 2 > 1$. Except for a few crRNA variants that retained weak activity, most crRNA variants with mutations at positions 3 or 4 exhibited an almost complete loss of *trans*-cleavage activity. This pattern aligns with the crRNA pseudoknot structure, as nucleotides at positions 3 and 4 are critical for pseudoknot formation and thus have the most significant effect on cleavage activity. In contrast, position 1, located at the 5′ end, likely contributes the least to pseudoknot stability, and thus had the smallest impact on *trans*-cleavage activity. To further validate the importance of the RRS, we sequentially truncated three mature crRNAs by removing 1–4 nucleotides from their 5′ ends (Supplementary Fig. 2). crRNA variants truncated by more than two nucleotides were almost completely inactivated, failing to produce fluorescence

https://doi.org/10.1038/s41467-025-62082-5

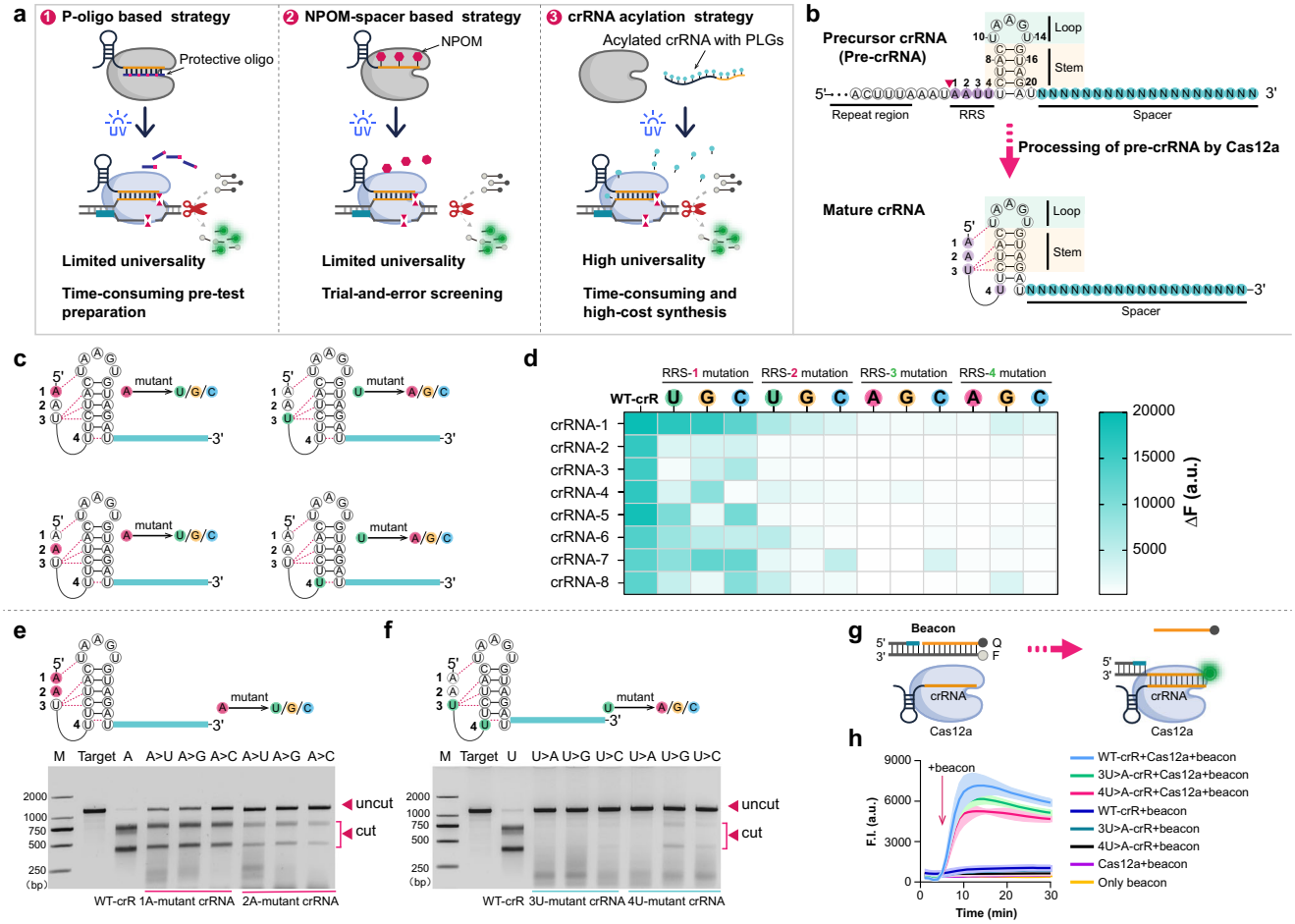


Fig. 1 | Identification of key nucleotides in the DR region of crRNA that influence Cas12a cleavage activity. a Schematic of three photo-controlled CRISPR-Cas12a activation strategies. **b** Schematic of Cas12a recognition of the RRS site and processing of pre-crRNA. **c** Schematic diagrams of single-base mutations at RRS positions 1–4. **d** Heatmap analysis of the effects of individual base mutations at the RRS 1–4 sites on the *trans*-cleavage activity of eight LbCas12a-crRNAs. ΔF represents the difference between the final fluorescence value and the initial fluorescence value. All experiments were performed in triplicate ($n = 3$), and the plotted data represent the mean values from three independent replicate experiments. **e** Agarose gel electrophoresis analysis of *cis*-cleavage activity of crRNA with single-base mutations at RRS positions 1 and 2. **f** Agarose gel electrophoresis analysis of *cis*-cleavage activity of crRNA with single-base mutations at RRS positions 3 and 4. For (**e**, **f**) all the experiments were performed three times. **g** Schematic diagram of the Cas12a beacon assay principle. Circles labeled F and Q represent fluorescent and quencher groups, respectively. **h** Fluorescence change curves after adding 500 nM beacon to different reaction systems. Error bars are presented as mean values +/- SD ($n = 3$). a.u. represents arbitrary units. Source data are provided as a Source Data file.

signals distinguishable from the negative control. This result reinforces the crucial role of RRS integrity in crRNA's *trans*-cleavage activity.

Additionally, we evaluated the effect of RRS site mutations on crRNA's *cis*-cleavage activity through gel electrophoresis. We selected crRNA-1 for in vitro *cis*-cleavage assays (Fig. 1e, f). crRNA-1 targets a 1000 bp dsDNA fragment, with expected *cis*-cleavage products of 624 bp and 376 bp. The results showed that single-base mutations at the four RRS positions affected *cis*-cleavage activity in a manner consistent with the *trans*-cleavage results. Furthermore, truncated crRNA variants also exhibited *cis*-cleavage activity that aligned with the *trans*-cleavage results (Supplementary Fig. 3). Taken together, these findings indicate that all four nucleotides in the RRS significantly influence both *cis*- and *trans*-cleavage activities of crRNA, with positions 3 and 4 being the most key sites.

Since single-base mutations at the RRS sites significantly affect crRNA cleavage activity, we hypothesize that this could be due to the inability of the mutated crRNA to form the correct secondary structure, thereby disrupting its binding with the Cas protein and target recognition. To test this hypothesis, we designed a molecular beacon-based assay[45] to evaluate the effect of RRS site mutations on the formation of the crRNA-Cas12a protein-target ternary complex. The beacon consists of three oligonucleotide segments: a 37-nt target strand (TS), a 20-nt non-target strand (NTS), and a 17-nt sequence containing the TTTA PAM site. These components anneal to form a nick-containing dsDNA. The target and non-target strands are labeled with a fluorescent dye and a quencher molecule, respectively. Due to energy transfer via FRET between the fluorescent and quencher groups, the initial fluorescence intensity of the beacon is low. When the Cas12a-crRNA complex binds to the beacon, it causes DNA strand dissociation, separating the fluorescent and quencher groups, leading to a significant increase in fluorescence intensity (Fig. 1g). As shown in Fig. 1h, when the beacon was added to CRISPR reaction systems containing crRNA variants with mutations at positions 3 and 4 (mutated to A), the fluorescence intensity rapidly increased, showing reaction rates comparable to the wild-type crRNA. In contrast, neither the crRNA nor the Cas protein alone could unwind the beacon. This result suggests that single-base mutations at the RRS sites do not affect the recognition and binding efficiency between crRNA, Cas12a, and the target. The observed effect on cleavage activity is likely due to structural changes in the protein during activation of the enzymatic activity. In comparison,

https://doi.org/10.1038/s41467-025-62082-5

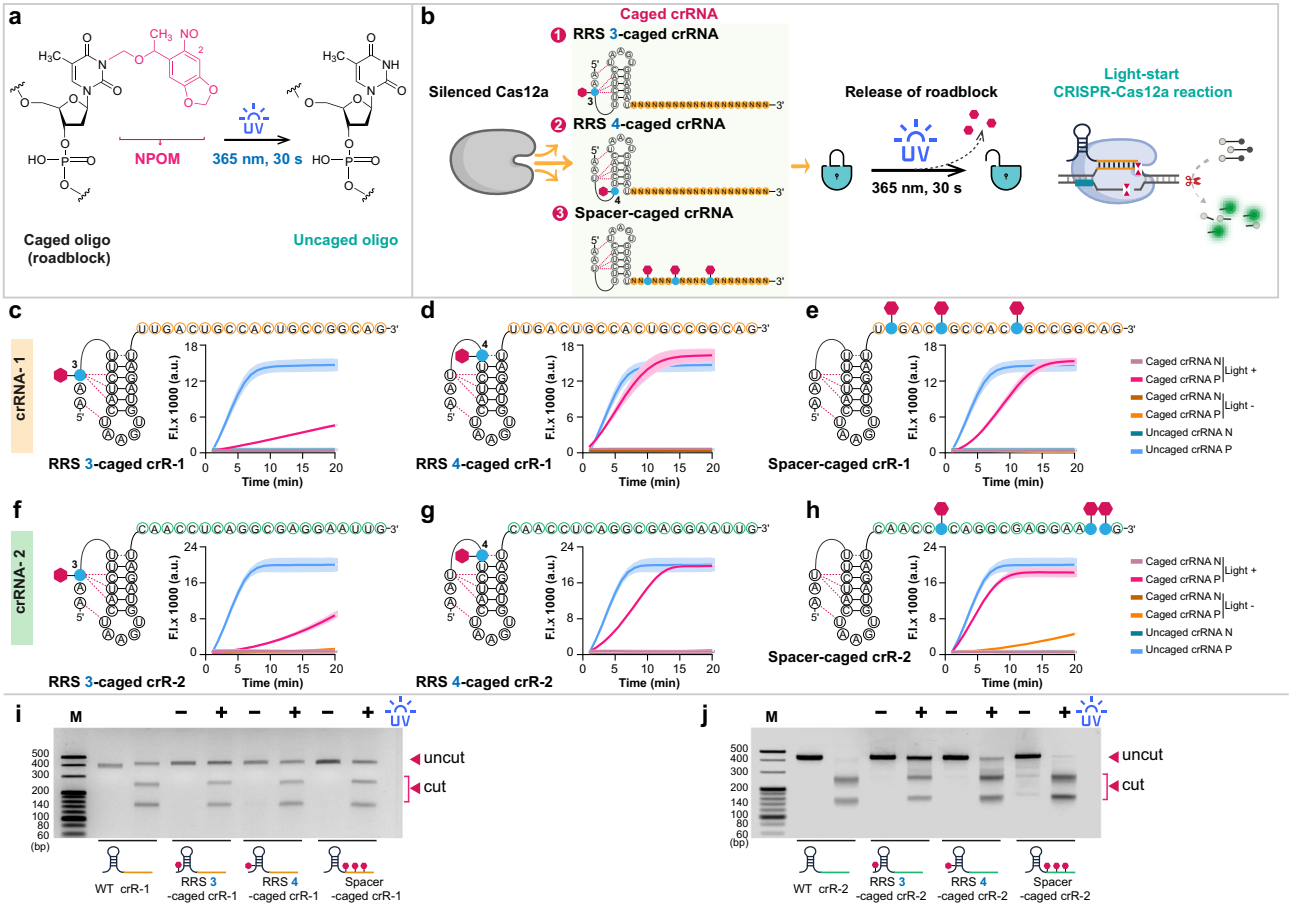


Fig. 2 | Development of the photo-controlled LbCas12a system with single-base photo-caging modifications. a Schematic of thymidine photo-caging through NPOM modification. NPOM modification is applied to the nitrogenous ring of thymidine, which is released from the thymidine upon exposure to 365 nm ultraviolet light for 30 seconds. **b** Schematic of photo-controlled Cas12a reactions mediated by three different crRNA photo-caging strategies. (1) NPOM photo-caging at the third position U of the RRS. (2) NPOM photo-caging at the fourth position U of the RRS. (3) NPOM photo-caging at three discontinuous bases in the spacer region. Blue circles represent photocaged thymidine, and magenta hexagons represent NPOM modification. **c** Inactivation and photo-regulated recovery of *trans*-cleavage activity mediated by RRS-3 single-base photocaged crRNA-1. **d** Inactivation and photo-regulated recovery of *trans*-cleavage activity mediated by RRS-4 single-base photocaged crRNA-1. **e** Inactivation and photo-regulated recovery of *trans*-cleavage activity mediated by crRNA-1 with photocaged three discontinuous bases in the spacer region. **f** Inactivation and photo-regulated recovery of *trans*-cleavage activity mediated by RRS-3 single-base photocaged crRNA-2. **g** Inactivation and photo-regulated recovery of *trans*-cleavage activity mediated by RRS-4 single-base photocaged crRNA-2. **h** Inactivation and photo-regulated recovery of *trans*-cleavage activity mediated by crRNA-2 with photocaged three discontinuous bases in the spacer region. Real-time fluorescence curves shown in panels (**c**–**h**) were continuously collected over 20 min, with a final target concentration of 1 nM in each reaction. All experiments were performed in triplicate, with error bars representing mean values +/- SD ($n = 3$). a.u. represents arbitrary units. crRNA-N serves as the non-target control, while crRNA-P represents the positive experimental group with 1 nM target DNA added. **i** Comparison of the inactivation and photo-regulated recovery of *cis*-cleavage activity mediated by different photocaged crRNA-1. **j** Comparison of the inactivation and photo-regulated recovery of *cis*-cleavage activity mediated by different photocaged crRNA-2. In the 3% agarose gel electrophoresis analysis shown in panels (**i**) and (**j**), unmodified wild-type crRNA was used as the control to compare *cis*-cleavage activity inactivation and photo-regulated recovery mediated by crRNA with photo-caging at the RRS-3, RRS-4, and spacer regions. The '+' and '–' symbols denote UV-irradiated and non-irradiated control groups, respectively. For (**i**, **j**), all the experiments were performed three times. Source data are provided as a Source Data file.

the truncated crRNA variants exhibited significantly slower reaction rates in the beacon assay than the wild-type crRNA, indicating that the complete loss of the RRS region impaired the recognition and binding between crRNA, Cas12a, and the target (Supplementary Fig. 4).

Development of a photo-controlled LbCas12a system with single-base caged modifications in crRNA

6-Nitropiperonyloxymethyl (NPOM) is a photosensitive protective group that can "cage" nucleotide bases, temporarily inactivating their function (such as base hybridization or target recognition)[46]. Upon exposure to ultraviolet light (365 nm), the caging group can be rapidly removed, restoring the biological function of the nucleotide (Fig. 2a). In our previous studies, to effectively control the activation and inactivation of CRISPR-Cas activity, we introduced three non-contiguous U bases within the first 15 nucleotides near the 5′ end of the spacer region and replaced them with NPOM-dT[39]. However, the position and number of photo-responsive groups on the spacer are often limited by the target nucleic acid sequence, requiring redesign and optimization of the entire photo-control system when the target sequence changes. Given our previous discovery of the critical importance of the third and fourth U bases in the RRS for crRNA activity, we propose replacing these two U bases with T bases modified with photo-caging groups. This could enable the development of a simple, spacer sequence-independent, and universal single-base photo-switching strategy. (Fig. 2b).

Subsequently, we applied photo-caging modifications to the RRS positions 3 and 4 of six crRNAs targeting different sequences to assess their inhibition and recovery upon UV light exposure. The recovery efficiency was evaluated using in vitro *trans*-cleavage fluorescence assays, and the results were compared to crRNAs with three NPOM-dT modifications in the spacer region (Fig. 2c–h and Supplementary Fig. 5). The experiments demonstrated that both single-base photo-caging strategies effectively inhibited crRNA activity. Upon UV exposure, the crRNA with modification at position 4 showed rapid and complete restoration of cleavage activity. However, the activity recovery effect of the crRNAs with modification at position 3 varies, crRNA-4 only recovered about 20% of its cleavage activity. For comparison, the crRNA with NPOM-dT modifications in the spacer region showed complete inhibition and effective recovery, consistent with previous studies (Fig. 2e). However, for crRNA-2, since the two U bases in the spacer region are located near the 3′ end, even replacing all three U bases with NPOM-dT modifications cannot fully deactivate its activity (Fig. 2h).

Further, we evaluated the *cis*-cleavage inhibition and recovery effects for these photo-caged crRNAs, and the results were consistent with the *trans*-cleavage reactions (Fig. 2i, j). In the unexposed experimental groups, crRNA-2 with spacer-region photo-caging failed to completely inhibit Cas12a's *cis*-cleavage activity. In contrast, other photo-caged crRNAs did not show any detectable cleavage bands. The photo-recovery effect of the *cis*-cleavage reaction differs between the two crRNAs. The weak baseline *cis*-cleavage activity of the wild-type crRNA-1 results in a less pronounced recovery effect after photo-caging removal, compared to the more noticeable effect observed in the *trans*-cleavage activity. For crRNA-2, the photo-recovery effect matched the *trans*-cleavage results. In the UV-exposed groups, except for the crRNA-2 with modification at position 3, which showed a faint cleavage band due to a more significant impact of NPOM on its *cis*-cleavage activity, the other modified crRNAs generated cleavage bands of similar intensity to the wild-type crRNA.

In summary, we found that single-base photo-caging at positions 3 and 4 of the crRNA RRS effectively blocked crRNA activity in the absence of UV treatment. However, the recovery at position 4 was notably more efficient than at position 3, with almost full activity restoration after rapid UV exposure. Consequently, we selected position 4 of the RRS as the optimal site for the single-base photo-regulated design. This single-base photo-caging strategy effectively addresses the need for meticulous optimization of modification positions and quantities in spacer-region photo-caging strategies. It offers greater versatility, simplifying the design process while significantly reducing sequence synthesis costs.

Split crRNA-mediated single-base photo-regulated strategy

Previous studies have shown that Cas12a can recruit split crRNA for target recognition and cleavage[15,47]. Split crRNA not only preserves detection performance comparable to full-length crRNA but also increases the design flexibility and versatility of the CRISPR-Cas system. Single-base photo-caging at position 4 of the RRS offers an easily designed, universal photo-regulated strategy. However, when changing detection targets, a new photocaged crRNA must still be synthesized. To further reduce crRNA synthesis costs and enhance the versatility of this single-base photo-caging strategy, the photocaged crRNA can be split into two parts. The 5′ end of the photocaged crRNA, containing the photo-caging modification, can be pre-synthesized as a universal sequence, while the 3′ end can be designed and synthesized as a variable sequence tailored to different target sequences.

We implemented two forms of crRNA splitting for LbCas12a: (a + b) represents splitting the crRNA into a 20-nt DR region and a 20-nt spacer; (c + d) represents splitting the crRNA at the stem-loop of the DR region, consisting of a 10-nt partially DR region and a shortened partially DR region along with the spacer region (a total of 26 nt) (Fig. 3a). We then compared the *trans*-cleavage ability of these two split crRNAs with the full-length crRNA in the detection of single-stranded and double-stranded targets (Fig. 3b, c). The results show that crRNA split at the stem-loop of the DR region maintains detection efficiency comparable to that of full-length crRNA for both kinds of target, indicating that this splitting method does not affect crRNA functionality. In contrast, crRNA split between the DR and spacer significantly reduced efficiency in detecting double-stranded DNA, which is unfavorable for building high-sensitivity detection systems. Therefore, subsequent experiments used crRNA split at the stem-loop of the DR. We further confirmed, through component knockout experiments, that both parts of the split crRNA are essential for target detection by the CRISPR-Cas system, consistent with previous findings (Supplementary Fig. 6). Additionally, we evaluated the impact of the two splitting methods on the detection efficiency of AsCas12a. Unlike LbCas12a, AsCas12a's crRNA, when split by either method, does not affect detection efficiency for both ssDNA and dsDNA target (Supplementary Fig. 7). However, due to the higher catalytic activity of LbCas12a compared to AsCas12a, LbCas12a was used in this study.

Next, we evaluated the sensitivity of stem-loop split crRNA for direct detection of double-stranded DNA targets, comparing it with the full-length crRNA (Fig. 3d-f). The experimental results showed that both the split crRNA and the full-length crRNA were capable of detecting targets at a final concentration of 1 pM, laying the foundation for using split crRNA in high-sensitivity detection. Finally, we performed single-base photo-caging at the RRS-4 position of the split crRNA (Fig. 3g). *Trans*-cleavage and *cis*-cleavage experiments confirmed that the single-base photo-caging strategy for the split crRNA achieved the same inhibition and recovery effects as the full-length crRNA (Fig. 3h, i). This development provides a more universal, cost-effective, and flexible strategy for photo-regulation of Cas12a activity.

Development of a photo-regulated one-pot Cas 12a system based on split crRNA

In previous work, we have developed a photo-controlled one-pot Cas12a system using NPOM-modified crRNA in the crRNA spacer region[39]. However, this approach requires meticulous optimization of crRNA design to ensure effective photo-caging modification of three non-contiguous U bases. In the present study, we applied a single-base photo-caging strategy to split crRNA, validated in earlier experiments, to develop a more versatile, cost-effective, and easily designed one-pot recombinase polymerase amplification (RPA)-LbCas12a system (Fig. 4a). In this system, the single-base photo-caging at position 4 of the RRS in split crRNA initially keeps the CRISPR-Cas system inactive. After efficient isothermal amplification of the target for 10 min, exposure to 365 nm UV light for 30 seconds removes the photo-caging group, thereby activating Cas12a to recognize the amplification products and perform *trans*-cleavage of the fluorescent reporter probe, resulting in the accumulation of detectable fluorescence signals.

To evaluate the detection performance of the one-pot RPA-LbCas12a detection system based on single-base photocaged split crRNA, we used *mycoplasma pneumonia* (MP) gene fragments with final concentrations of 1 fM, 100 aM, 10 aM, 1 aM, and 0.1 aM as targets to assess the detection limit (Fig. 4b). The results showed that the detection sensitivity of the single-base photocaged split crRNA system was comparable to that of the spacer photo-caging strategy, with both systems capable of detecting double-stranded DNA targets as low as 1 aM (Fig. 4b, c and Supplementary Fig. 8). We next validated that the system not only ensures high sensitivity but also offers greater flexibility in target selection and universality. Since the photocaged single base is located in the DR region of the split crRNA, it can serve as a universal, pre-prepared reagent. This allows it to be paired with any spacer sequence synthesized according to different target sequences, making the approach highly adaptable. To demonstrate such an application, we selected five pathogens—SARS-CoV-2, Epstein-Barr

https://doi.org/10.1038/s41467-025-62082-5

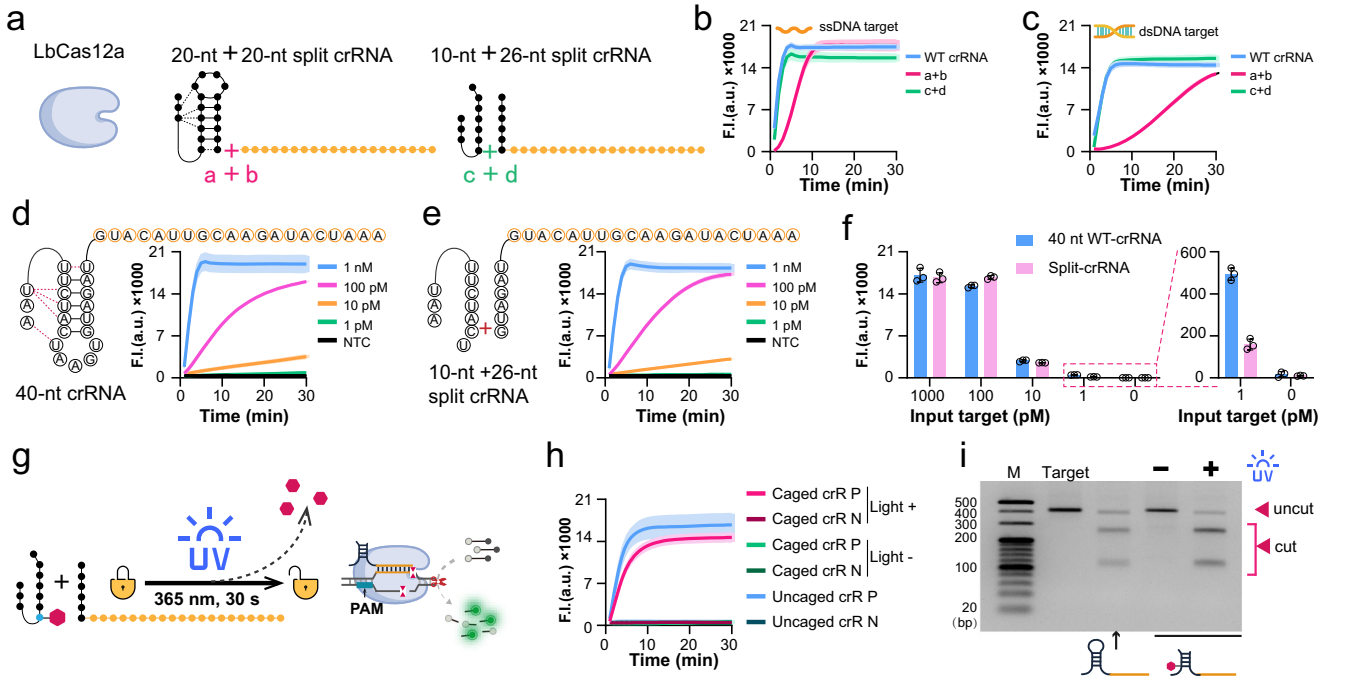


Fig. 3 | Split crRNA-mediated photo-regulated strategy. a Schematic diagram of two split strategies for LbCas12a crRNA. **b** Real-time fluorescence signal curves for the detection of ssDNA targets by two types of split crRNAs. Full-length (40-nt) WT-crRNA was used as a positive control. **c** Real-time fluorescence signal curves for the detection of dsDNA targets by two types of split crRNAs. Full-length (40-nt) WT-crRNA was used as a positive control. In panels (**b**, **c**) the target concentration was 1 nM for both. All experiments were performed in triplicate. Error bars represent the mean values +/- SD ($n = 3$). **d** Real-time fluorescence curve for sensitivity detection using full-length (40-nt) crRNA. **e** Real-time fluorescence curve for sensitivity detection using stem-loop split crRNA. In panels (**d**, **e**) double-stranded targets were serially diluted with final concentrations of 1 nM, 100 pM, 10 pM, and 1 pM. **f** Comparison of sensitivity detection using full-length crRNA and stem-loop split crRNA. Endpoint fluorescence signals for each target concentration in (**d**, **e**) were normalized, where ΔF represents the final fluorescence value minus the initial fluorescence value. All experiments were performed in triplicate. Error bars represent the mean values +/- SD ($n = 3$). **g** Schematic diagram of the Photo-regulated strategy mediated by RRS-4 single-base photocaged split crRNA in the CRISPR-Cas12a system. **h** *Trans*-cleavage activity blockade and photo-recovery experiment mediated by RRS-4 single-base photocaged split crRNA. Real-time fluorescence curves shown in (**h**) were continuously collected over 30 min. Target concentration in each reaction system was 1 nM, and all experiments were performed in triplicate. Error bars represent the mean values +/- SD ($n = 3$). a.u. represents arbitrary units. **i** Agarose gel electrophoresis experiment characterizing *cis*-cleavage activity blockade and photo-recovery mediated by RRS-4 single-base photocaged split crRNA, with unmodified full-length WT-crRNA as a control. The '+' and '−' symbols denote UV-irradiated and non-irradiated control groups, respectively, all the experiments were performed three times. Source data are provided as a Source Data file.

Virus (EBV), Human Papillomavirus Type 18 (HPV18), MP, and Human Adenovirus Type 7 (HAdV7)—as test targets and performed sensitivity experiments. The results showed that the detection limit for all five targets reached 1 aM (Fig. 4d–h and Supplementary Fig. 9). These findings demonstrate that the single-base photocaged split crRNA one-pot system not only achieves detection sensitivity comparable to the spacer photo-caging strategy but also overcomes its limitations in target sequence selection, providing enhanced versatility, simplified design, and reduced costs.

Evaluation of the clinical detection performance of the split crRNA-mediated Photo-controlled CRISPR detection technique

After validating the detection sensitivity and universality of the photo-controlled one-pot CRISPR system based on split crRNA, we next evaluated its clinical performance using *MP* as the target (Fig. 5a). *MP* is a common pathogen that causes respiratory infections in humans. It is transmitted through close contact and can lead to periodic regional outbreaks[48]. Thus, developing a rapid and accurate screening method is essential for early intervention and controlling the spread of the pathogen. For this evaluation, we designed RPA amplification primers and single-base photocaged crRNA targeting the P1 gene of *MP*. We collected 35 throat swab samples from patients suspected of *MP* infection and extracted nucleic acids using a standardized extraction system. The samples were also tested using both the single-base photocaged full-length crRNA-mediated one-pot system (Fig. 5b) and the split crRNA-mediated photo-controlled one-pot system (Fig. 5c). The results showed that the full-length photo-caged crRNA-mediated one-pot system detected 30 positive samples, with the highest *Ct* value of 36.09 (Sample ID 35). The single-base photocaged split crRNA-mediated one-pot system detected 29 positive samples, with the highest *Ct* value of 35.06 (Sample ID 19). Both methods exhibited 100% specificity, with no false positives observed (Fig. 5b–d).

The clinical samples used in the previous experiments required multi-step, time-consuming nucleic acid extraction. To streamline the process and reduce the turnaround time from sample input to result output, we implemented a rapid nucleic acid release protocol using Chelex-100 resin[49], completing the procedure in just two minutes. To further eliminate reliance on large, specialized laboratory equipment, we employed a previously developed portable, photo-controlled fluorescence detection instrument[39] for the entire workflow, including the photo-controlled one-pot reaction and signal acquisition (Fig. 5e). To evaluate the performance of this streamlined workflow and portable instrument for clinical sample detection, we collected 14 throat swab samples from individuals suspected of *MP* infection. After rapid thermal lysis for nucleic acid release, the samples were analyzed using both a professional fluorescence quantitative PCR instrument and the portable device. As shown in Fig. 5f, the portable device successfully detected 9 positive and 5 negative samples, achieving 100% sensitivity and specificity. The total turnaround time from sample input to result was ~20 min. The real-time fluorescence curves from the portable device were highly consistent with those obtained using the

https://doi.org/10.1038/s41467-025-62082-5

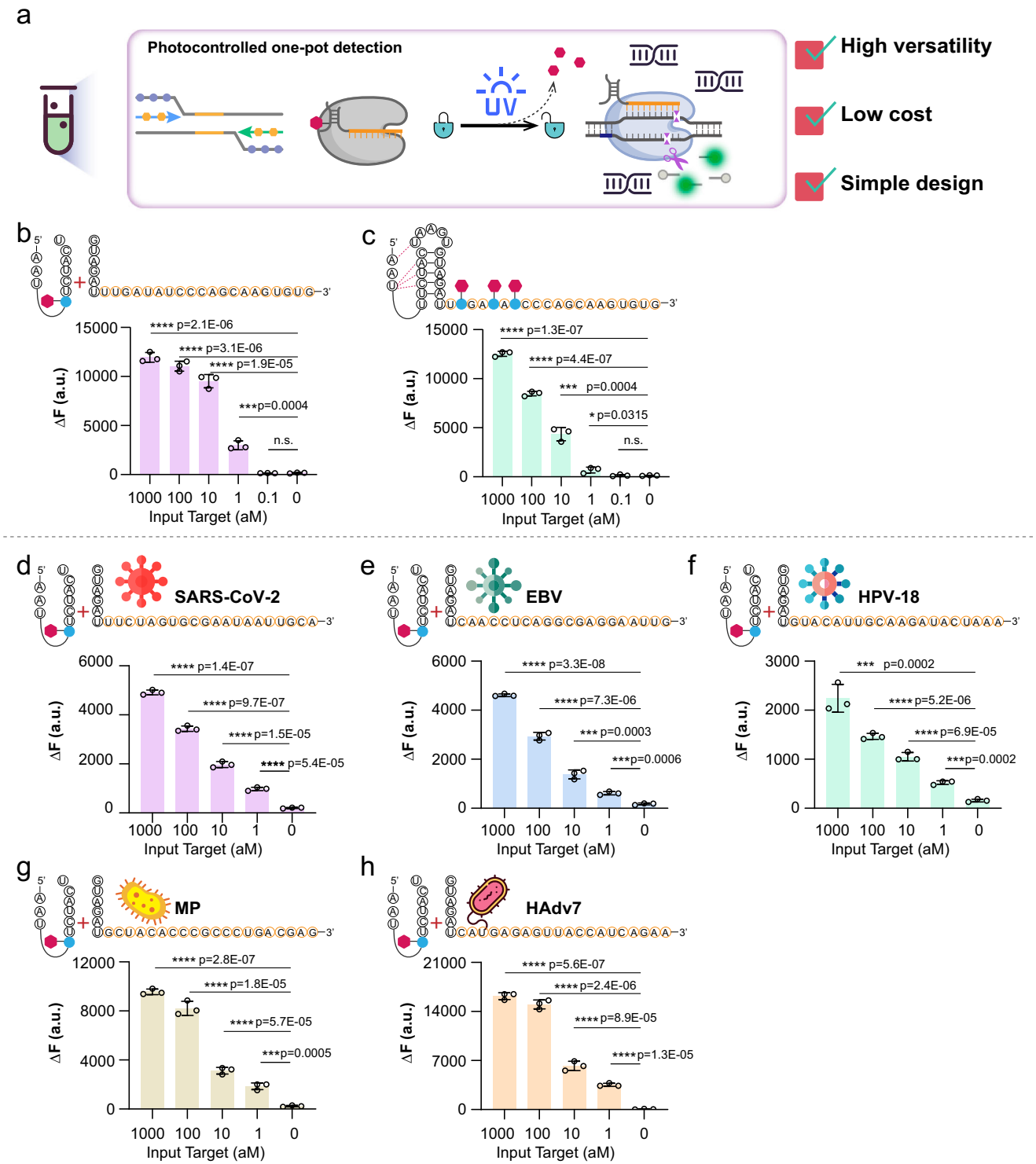


Fig. 4 | Sensitivity and universality assessment of the split crRNA-mediated one-pot RPA-LbCas12a photo-controlled system. a Schematic diagram of the RRS-4 single-base photocaged split crRNA-mediated one-pot detection system. **b** Sensitivity analysis of the photo-controlled one-pot system mediated by RRS-4 single-base photocaged split crRNA. **c** Sensitivity analysis of the photo-controlled one-pot system mediated by spacer region photo-caged full-length crRNA. In (**b**, **c**) double-stranded targets were serially diluted to final concentrations of 1 fM, 100 aM, 10 aM, and 0.1 aM. **d**–**h** Universality validation of the RRS-4 single-base photocaged split crRNA-mediated photo-controlled one-pot system. **d** Sensitivity analysis for detection of the SARS-CoV-2 spike gene. **e** Sensitivity analysis for detection of EBV. **f** Sensitivity analysis for detection of HPV-18. **g** Sensitivity analysis for detection of *Mycoplasma pneumoniae* (MP). **h** Sensitivity analysis for detection of *HAdV7*. DNA targets used in (**d**–**h**) were PCR products amplified from synthetic plasmid genomes (SARS-CoV-2) and pathogenic microbial genomes (EBV, HPV-18, MP, HAdv7) extracted from clinical samples. These products were purified by gel extraction and quantified using Qubit. ΔF represents the difference between the final fluorescence value and the initial fluorescence value. All experiments were performed in triplicate, with error bars representing the mean values +/- SD ($n = 3$), and statistical analysis was conducted using a two-tailed *t*-test. Statistical significance is indicated as follows: *n.s.* no significance with $P > 0.05$, and the asterisks (* $P < 0.05$; ** $P < 0.01$; *** $P < 0.001$; **** $P < 0.0001$.). a.u. represents arbitrary units. Source data are provided as a Source Data file.

professional fluorescence quantitative PCR instrument (Supplementary Fig. 10).

Discussion

The development of one-pot CRISPR detection systems is essential for advancing CRISPR-based diagnostic technologies[6,7]. Currently, most one-pot CRISPR detection methods aim to weaken the cleavage activity of the CRISPR-Cas system to minimize interference with isothermal amplification during the early stages of the reaction[30–32]. However, this balance between amplification and CRISPR-Cas cleavage often comes at the expense of detection efficiency. In contrast, photo-controlled methods can completely silence enzyme activity, thereby avoiding interference with nucleic acid amplification[37–40]. Once amplification is complete, light can reactivate the enzyme activity to near its original level, preserving the efficiency of subsequent detection.

In this study, we further refine the previously developed photo-controlled CRISPR technology to overcome its limitation of restricted universality. Previous approaches focused on regulating the spacer region of crRNA, which required reconfiguration of the caging strategy based on the target sequence. For instance, the number and position of photocaged sites, modified with the NPOM group, can significantly influence both the caging effect and activity restoration. Additionally, current chemical modifications are typically effective only for T (U) bases, while modifying A, C, and G bases is more challenging. This complicates the design strategy, as the number of U bases in spacer region of different crRNAs varies. Identifying crRNA modifications with optimal performance is both time-consuming and costly. Therefore, developing a photo-controlled CRISPR detection strategy that does not rely on alterations to the target sequence will be crucial for its widespread application.

The LbCas12a system, one of the most commonly used Cas12a variants, features a 20-bp sequence in the DR of its crRNA[50]. This DR sequence is conserved in the system, and any structural changes within the DR region result in the loss of activity. Therefore, regulating its activity through the DR region is a potentially universal approach. Identifying the specific sites critical for its cleavage activity is essential, especially to determine whether modifications at a single site can toggle activity. Such findings would facilitate easier modifications of the system. The DR region can be structurally divided into three parts: the loop, stem, and RRS regions. Previous studies have shown that the loop region is not essential for LbCas12a activity, as the enzyme retains its activity even without the loop after the crRNA is split[51]. The stem region helps maintain the stable pseudoknot structure, which is relatively complex, making it difficult to assess how a single-base change impacts its stability. On the other hand, the four-base RRS region has been shown to be highly sensitive to the processing of precursor crRNA by Cas12a, with even a single-base change leading to a near-complete loss of processing activity[42].

Based on this, we first performed mutation analysis of the four bases in the RRS region. Interestingly, we discovered that mutations at the 3rd or 4th base alone were sufficient to abolish both *cis*- and *trans*-cleavage activities. It is surprising that a single-base change has such a profound effect on crRNA activity. Our findings suggest that these two mutated crRNAs are still capable of mediating the binding, recognition, and unwind of double-stranded DNA by LbCas12a. Notably, this dissociation is not due to direct hybridization between the crRNA spacer region and DNA, as the absence of LbCas12a does not produce signal. Therefore, the loss of cleavage activity likely involves a distinct mechanism, which warrants further investigation.

After identifying two key sites, we next evaluated whether NPOM cage modification at these sites would also lead to a loss of activity. NPOM caging of the T (U) base can obstruct hydrogen bond formation, thereby losing its pairing ability. Structural studies have shown that the RRS region stabilizes the crRNA structure by forming intramolecular interactions with other bases in the DR region. For example, in this study, we identified a key base in the RRS region, the U (+4) base, which was previously observed by cryo-electron microscopy to pair with the U (+20) base in the DR region. The U (+3) base in the RRS region is deeply embedded in the center of the stem-loop, forming hydrogen bonds with A (+8), U (+7), and C (+6) in the stem-loop[52]. Since these two bases are critical for pseudoknot structure formation, we hypothesize that modification at these positions would disrupt this stable structure, leading to an impact on activity. As confirmed in our previous experiments, both sites exhibited photo-regulated capabilities. However, it appears that NPOM caging of the U (+4) base completely blocks the cleavage activity, achieving a detection efficiency comparable to that of uncaged crRNA once activated by light. Based on these findings, we conclude that single-base modifications in the crRNA DR region can efficiently mediate the on-off switching of LbCas12a activity through rapid light regulation. This performance is comparable to the crRNA spacer modification strategy.

Furthermore, we explored whether this single-base-mediated photo-regulation is applicable to the split crRNA design. It has been demonstrated that split of full-length crRNA still retains significant cleavage activity. Our results show that using a 10 + 26 nt split crRNA strategy can achieve detection efficiency comparable to that of the full-length crRNA. Interestingly, the same U (+4) base-mediated photo-regulation strategy continues to function effectively within this split crRNA system. This finding led us to develop a more versatile CRISPR photo-controlled one-pot system, which has been shown to efficiently detect targets from five different pathogens. Since the modification of photocaged bases is fixed to a specific sequence and can be prepared in large quantities in advance, replacing a target for detection can be done using the same reagents, significantly reducing synthesis and modification costs. We expected that this universal light activation strategy could also be applied to multi-crRNA detection approaches, enhancing the signal-to-noise ratio in photo-controlled single-molecule droplet assays.

Our clinical analysis of *MP* samples demonstrated that, whether using the full-length crRNA strategy or the split crRNA strategy, the single-base photo-controlled one-pot CRISPR method can effectively detect samples with *Ct* values as high as 35. The detection efficiency is comparable to the spacer sequence-based regulation method we previously developed. This approach could be applied to point-of-care testing (POCT) diagnostics, as evidenced by our preliminary validation of a reliable, full-process method for detecting *MP*, which involves a 2-min sample processing step and ~15–20 min for one-pot CRISPR detection.

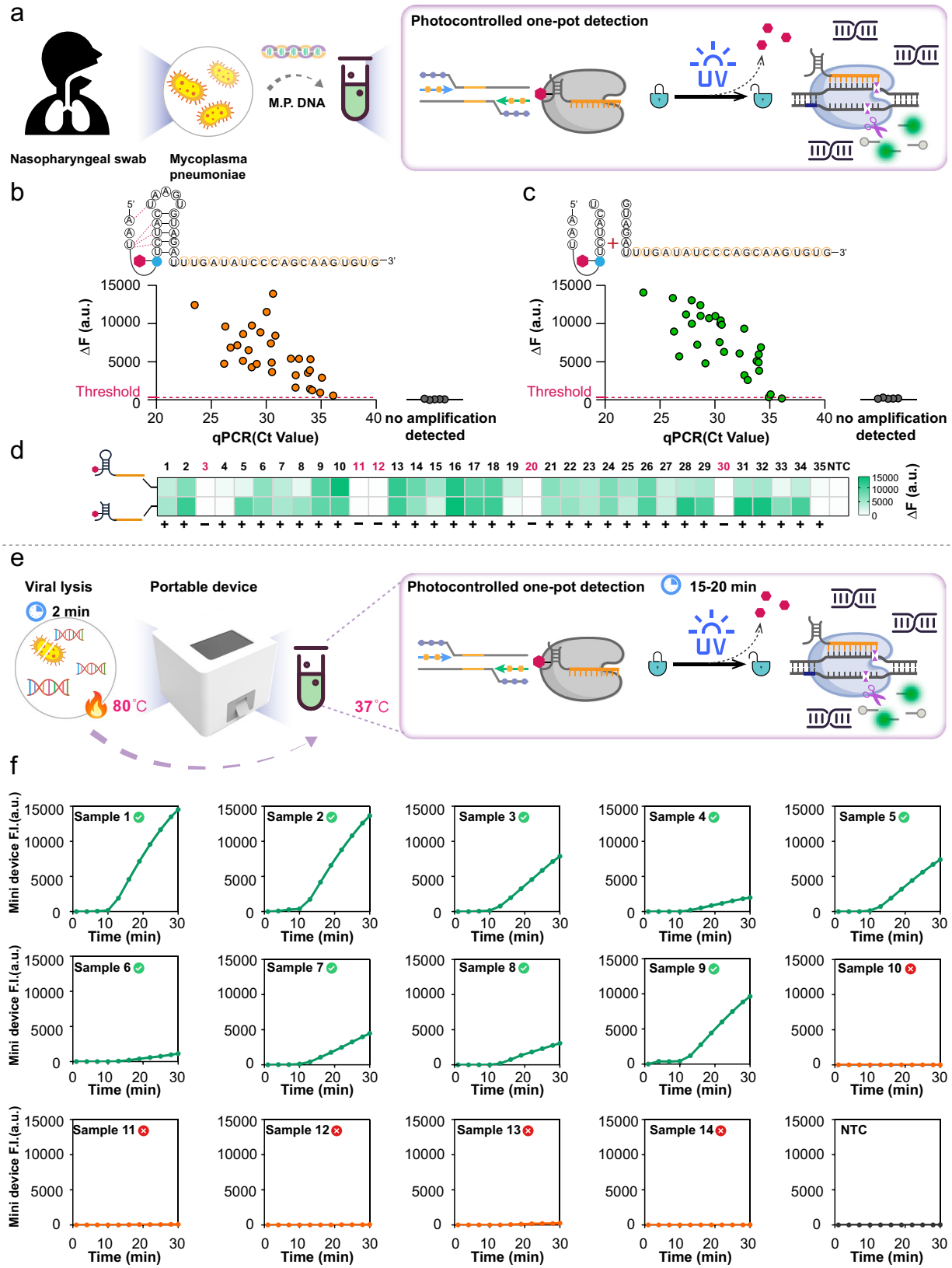
Furthermore, although this study primarily focuses on the design and validation of crRNAs for LbCas12a, we hypothesize that, given the conserved RRS present in various Cas12a homologs[51], the single-base photocaged strategy developed in this study may also be applicable to other Cas12a homologs. It is also important to note that, while our research is centered on the application of CRISPR diagnostics, this more universal photo-controlled strategy can be extended to the gene editing field.

Methods

Ethical statement

Clinical samples for this research were collected from patients who visited the first hospital of Guangzhou medical university for routine diagnosis and treatment. All participants provided informed consent prior to sample collection, demonstrating a full understanding of the study's purpose, procedures, and potential risks. Participants' personal information will be maintained in strict confidentiality, and all data will be processed anonymously to ensure the protection of their privacy. The clinical samples were collected with informed consent and were fully de-identified prior to analysis. No

https://doi.org/10.1038/s41467-025-62082-5



demographic information, including sex, gender identity, or age, was linked to the samples. As a result, sex and/or gender were not considered in the study design or data analysis, in accordance with the SAGER guidelines. The research protocol was performed following the guidelines approved by Ethics Committee of (approval ID: 2021-K-40).

Materials

All the DNA sequences were synthesized by Sangon (Shangai, China), all RNA sequences, were synthesized by Hippo Biotechnology (Huzhou, China), detailed sequence information is provided in Supplementary Table 1-6 and Supplementary Data 1. The RPA kit was purchased from Amplification Future Biotechnology (Changzhou,

Fig. 5 | Clinical applicability assessment of the split crRNA-mediated photo-controlled one-pot CRISR system for MP detection. a Schematic of the RRS-4 single-base photocaged split crRNA-mediated one-pot system for clinical detection of *MP*. **b** Scatter plot showing clinical *MP* detection using the RRS-4 single-base photocaged full-length crRNA-mediated one-pot system. **c** Scatter plot showing clinical *MP* detection using the RRS-4 single-base photocaged split crRNA-mediated one-pot system. Orange and green points represent *MP*-positive clinical samples identified by qPCR, while gray points represent negative samples. The threshold line (red dashed line) indicates the average fluorescence value of negative samples plus three standard deviations. **d** Heatmap of clinical *MP* detection using both the RRS-4 single-base photocaged full-length and split crRNA-mediated one-pot systems. ΔF represents the difference between the final and initial fluorescence values. **e** Workflow for on-site *MP* detection using the RRS-4 single-base photocaged split crRNA-mediated one-pot system with a portable device. **f** Real-time fluorescence curves for the detection of 14 clinical *MP* nasopharyngeal swab samples using the portable device. a.u. represents arbitrary units. Source data are provided as a Source Data file.

China, catalog number: WLB8201KIT). The Cas12a and reaction buffer were obtained from Bio-lifesci (Guangzhou, China, catalog number: M20301-0500). Biowest Agarose was purchased from Baygene Biotechnology (Shanghai, China, catalog number: BY-R0100). E.Z.N.A® Gel Extraction kit was purchased from Omega Bio-Tek (USA, catalog number: D2500-03). Qubit™ 1× dsDNA HS (High Sensitivity) Assay kit was purchased from Thermo Fisher scientific (USA, catalog number: Q33231). The *mycoplasma pneumoniae* qPCR kit was obtained from Rongjin Technology (Shenzhen, China, catalog number: RN216FP). Chelex 100 resin was purchased from Bio-Rad Laboratories (USA, catalog number: 1421253).

Preparation of dsDNA targets

The 50 μL PCR reaction system for dsDNA targets preparation comprised 1× PrimeSTAR® HS Premix (Takara, Japan, catalog number: R040A), 200 nM forward primer, 200 nM reverse primer, and 1 ng plasmid target or 1 μL clinical sample. The PCR procedure consisted of the following steps: initial denaturation at 98 °C for 1 min; denaturation at 98 °C for 10 s, annealing at 55 °C for 5 s, and extension at 72 °C for 30 s (extension time adjusted according to the length of the target fragment, at a rate of 1 kb/min), repeated for a total of 30 cycles; followed by a final extension at 72 °C for 5 min. The PCR products were purified and recovered using the E.Z.N.A® Gel Extraction kit. The final products were accurately quantified with a Qubit 4.0 fluorometer (Thermo Fisher Scientific, USA, catalog number: Q33231), aliquoted, and stored at −20°C for subsequent use.

The plasmids or clinical samples used in the PCR reaction were sourced as follows: the SARS-CoV-2 S gene plasmid and EBV (Epstein-Barr virus) plasmid were synthesized by Tsingke Biotechnology (Shanghai, China). Clinical Nasopharyngeal swab samples of HPV-18 (Human Papillomavirus), HAdv7 (Human adenovirus), and MP (*Mycoplasma Pneumoniae*) were collected from the First Hospital of Guangzhou Medical University, and genomic DNA was extracted using the P2 biosafety laboratory automated extraction platform. All procedures were approved by the Ethics Committee of the First Hospital of Guangzhou Medical University.

Preparation of NPOM-caged crRNA

The NOPM-caged crRNA sequences mentioned in the manuscript were chemically synthesized by Hippobiotec (Huzhou, China) using a Dr. Oligo 48 DNA/RNA Synthesizer (Biolytic, USA) with a standard CPG solid-phase support. The commonly used monomers for automated RNA synthesis were obtained from Hongene Biotech (Shanghai, China, catalog number: HP02568), while the NPOM-caged-dT CE-Phosphoramidite was prepared by Hippobiotec (Huzhou, China, catalog number: HP30750). For the synthesis of the conventional bases, standard synthesis cycles were used, with a coupling time of 2 min. For the incorporation of the caged-dT modification, the coupling time was extended to 10 min. The reaction progress was monitored by tracking the amount of dimethoxytrityl (DMT) cation released after each deprotection step. Upon completion of the standard RNA synthesis process, the RNA product was cleaved from the CPG support and treated with a 22% ammonium hydroxide solution at room temperature for 12 h. The oligonucleotide was then recovered by ethanol precipitation and dissolved in a mixture of anhydrous DMSO and TEA.3HF (volume ratio 1:1.25), followed by heating at 65 °C for 2.5 h.

Purification was carried out using an Agilent 1260 system with a PLRP-S column (250 mm × 4.6 mm, 100 Å, 5 μm). The mobile phase A was 100 mM TEAA (triethylammonium acetate) buffer containing 50% acetonitrile, while mobile phase B was 100 mM TEAA. The oligonucleotide was eluted using a gradient of 15%–60% mobile phase A over 60 min, with a flow rate of 1 mL/min. After purification, the product was lyophilized and desalted using Bio-Rad's Bio-Spin 6 columns. Finally, the purified product was dissolved in TEPC-treated water and stored at −80 °C for subsequent experiments.

In Vitro CRISPR-Cas12a *trans*-cleavage assay

The 20 μL reaction system consisted of 1× Cas12a reaction buffer, 120 nM LbCas12a or AsCas12a, 100 nM crRNA, 500 nM FAM-6C-BHQ1, and 2 μL DNA target. The reaction was carried out at 37 °C for 30 min. The TaKaRa TP950 Real-Time System III was utilized for thermostated reactions and the real-time acquisition of FAM fluorescence signal, with data points collected at one-min intervals.

In Vitro CRISPR-Cas12a *cis*-cleavage assay

The 7 μL reaction system was prepared as follows: 1× Cas12a reaction buffer, 500 nM LbCas12a, 500 nM crRNA, and 80 ng dsDNA target. The reaction was incubated at 37 °C for 10 min, followed by denaturation at 95 °C for 20 min. The results of *cis*-cleavage were finally analyzed by 3% agarose gel electrophoresis.

Beacon assay

The main reagents used in this experiment are as follows: 10× annealing buffer (200 mM Tris-HCl, 100 mM NaCl, pH 7.5); 10× binding buffer (200 mM Tris-HCl, 500 mM NaCl, 1 mM DTT, 50 mM $MgCl_2$, pH 7.5). Firstly, Beacon dsDNA was obtained through an annealing reaction. The 50 μL annealing reaction system comprised 1× annealing buffer, 5 μM each of Beacon-17nt, Beacon-FAM, and Beacon-BHQ ssDNA sequences. The reaction program was set as follows: 90 °C for 5 min, followed by a gradual decrease to 20 °C at a rate of 2 °C per step, with each temperature held for 30 s, and a final hold at 20 °C for 3 min. Subsequently, the binding reaction of Beacon with Cas12a was performed. The 20 μL reaction system was prepared as follows: 1× binding buffer, 500 nM LbCas12a, 500 nM crRNA, and 500 nM Beacon dsDNA. The reaction was carried out at 37 °C for 30 min in the TaKaRa TP950 Real-Time System III, and the FAM fluorescence signal was collected at one-min intervals.

Photo-controlled RPA-LbCas12a one-pot assay

The 30 μL one-pot reaction system consisted of 1× Cas12a reaction buffer, 240 nM LbCas12a, 100 nM full-length crRNA or 1 μM split crRNA, 1 μM FAM-6C-BHQ1, 250 nM RPA forward primer, 250 nM RPA reverse primer, 11.8 μL RPA buffer A, 1 μL RPA buffer B, and 3 μL dsDNA target or clinical sample. The mixture was incubated at 37 °C for 10 min in the TaKaRa TP950 Real-Time System III. Subsequently, the program was paused, and the reaction tube was taken out and irradiated with an LED ultraviolet lamp (λ = 365 nm, 35 W) for 30 s before being returned to the instrument to continue the reaction for 60 min, during which the FAM fluorescence signal was collected at one-min intervals. For

experiments using a portable device for signal acquisition, there was no need to take out the reaction tube, as UV irradiation could be performed directly within the device.

Heat-lysed extraction of clinical MP samples

Firstly, the sample lysis reagent was prepared as follows: 50 mM DTT, 20% Chelex 100 resin (w/v), and TE buffer (pH 8.0). Subsequently, 25 μL of the sample lysis reagent was mixed with 25 μL of clinical MP sample, and incubated at 80 °C for 2 min. The lysate was stored at −80 °C.

Analysis of clinical MP samples by qPCR

The qPCR reaction system contained 18.5 μL PCR reaction premix, 1.5 μL PCR Polyase mixture, and 10 μL clinical MP sample. The qPCR program was set as follows: dUTP-UNG enzyme reaction at 50 °C for 3 min; initial denaturation at 95 °C for 2 min; 95 °C for 5 s, 60 °C for 35 s (signal acquisition), and 72 °C for 5 s, repeated for a total of 45 cycles. The FAM and ROX fluorescence signals were simultaneously collected using the QuantStudio™ 5.0 Real-Time PCR System (Thermo Fisher Scientific, USA), where the FAM fluorescence signal represented the clinical MP sample and the ROX signal represented the internal reference gene. The positive criteria of this qPCR kit was claimed as: ROX 16 $\leq Ct \leq 37$ and FAM $Ct \leq 37$. The Ct values of 35 clinical MP samples measured by qPCR were present in Supplementary Table 7.

Statistics and reproducibility

No statistical method was used to predetermine sample size. No data were excluded from the analyses. The experiments were not randomized. The investigators were not blinded to allocation during experiments and outcome assessment.

Reporting summary

Further information on research design is available in the Nature Portfolio Reporting Summary linked to this article.

Data availability

All data supporting the conclusions of this study are included in the main text and Supplementary Information. Source data are provided with this paper.

References

1. Adli, M. The CRISPR tool kit for genome editing and beyond. *Nat. commun.* **9**, 1911 (2018).
2. Pickar-Oliver, A. & Gersbach, C. A. The next generation of CRISPR–Cas technologies and applications. *Nat. rev. Mol. cell bio.* **20**, 490–507 (2019).
3. Wang, J. Y. & Doudna, J. A. CRISPR technology: a decade of genome editing is only the beginning. *Science* **379**, eadd8643 (2023).
4. Pardee, K. et al. Rapid, low-cost detection of Zika virus using programmable biomolecular components. *Cell* **165**, 1255–1266 (2016).
5. Zuo, X., Fan, C. & Chen, H.-Y. Biosensing: CRISPR-powered diagnostics. *Nat. Biomed. Eng.* **1**, 1–2 (2017).
6. Kaminski, M. M., Abudayyeh, O. O., Gootenberg, J. S., Zhang, F. & Collins, J. J. CRISPR-based diagnostics. *Nat. Biomed. Eng.* **5**, 643–656 (2021).
7. Tian T. & Zhou X. CRISPR-based biosensing strategies: technical development and application prospects. *Annu. Rev. Anal. Chem.* **16**, 311–332 (2023).
8. Liu, L. et al. The molecular architecture for RNA-guided RNA cleavage by Cas13a. *Cell* **170**, 714–726 (2017).
9. Chen, J. S. et al. CRISPR-Cas12a target binding unleashes indiscriminate single-stranded DNase activity. *Science* **360**, 436–439 (2018).
10. Li, S.-Y. et al. CRISPR-Cas12a has both cis-and trans-cleavage activities on single-stranded DNA. *Cell Res.* **28**, 491–493 (2018).
11. Gootenberg, J. S. et al. Nucleic acid detection with CRISPR-Cas13a/C2c2. *Science* **356**, 438–442 (2017).
12. Fuchs R. T., Curcuru J., Mabuchi M., Yourik P. & Robb G. B. Cas12a trans-cleavage can be modulated in vitro and is active on ssDNA, dsDNA, and RNA. Preprint at *BioRxiv*, https://doi.org/10.1101/600890 (2019).
13. Wu, X. et al. LbuCas13a directly targets DNA and elicits strong *trans*-cleavage activity. *Nat. Biomed. Eng*. https://doi.org/10.1038/s41551-025-01424-6 (2025).
14. Rananaware, S. R. et al. Programmable RNA detection with CRISPR-Cas12a. *Nat. commun.* **14**, 5409 (2023).
15. Chen, Y. et al. Split crRNA with CRISPR-Cas12a enabling highly sensitive and multiplexed detection of RNA and DNA. *Nat. commun.* **15**, 8342 (2024).
16. Li, J. et al. Discovery of the Rnase activity of CRISPR–Cas12a and its distinguishing cleavage efficiency on various substrates. *Chem. Commun.* **58**, 2540–2543 (2022).
17. Zhang, J. et al. Intrinsic RNA targeting triggers indiscriminate DNase activity of CRISPR-Cas12a. *Angew. Chem. Int. Ed.* **63**, e202403123 (2024).
18. Broughton, J. P. et al. CRISPR–Cas12-based detection of SARS-CoV-2. *Nat. biotechnol.* **38**, 870–874 (2020).
19. Kellner, M. J., Koob, J. G., Gootenberg, J. S., Abudayyeh, O. O. & Zhang, F. SHERLOCK: nucleic acid detection with CRISPR nucleases. *Nat. protoc.* **14**, 2986–3012 (2019).
20. Welch, N. L. et al. Multiplexed CRISPR-based microfluidic platform for clinical testing of respiratory viruses and identification of SARS-CoV-2 variants. *Nat. med.* **28**, 1083–1094 (2022).
21. Zhu, H. et al. PCR past, present and future. *Biotechniques* **69**, 317–325 (2020).
22. Chen, L., Hu, M. & Zhou, X. Trends in developing one-pot CRISPR diagnostics strategies. *Trends Biotechnol.* **43**, 98–110 (2025).
23. Chen, Y., Mei, Y., Zhao, X. & Jiang, X. Reagents-loaded, automated assay that integrates recombinase-aided amplification and Cas12a nucleic acid detection for a point-of-care test. *Anal. chem.* **92**, 14846–14852 (2020).
24. Wang, B. et al. Cas12aVDet: a CRISPR/Cas12a-based platform for rapid and visual nucleic acid detection. *Anal. chem.* **91**, 12156–12161 (2019).
25. Xu, Z. et al. Microfluidic space coding for multiplexed nucleic acid detection via CRISPR-Cas12a and recombinase polymerase amplification. *Nat. Commun.* **13**, 6480 (2022).
26. Li, H., Xiu, L., Guo, X., Hu, Q. & Yin, K. Spatiotemporal dual-dimensional separation enables ultra-simple one-pot CRISPR-based molecular diagnostics. *Chem. Eng. J.* **482**, 148872 (2024).
27. Lin, M. et al. Glycerol Additive Boosts 100-fold Sensitivity Enhancement for One-Pot RPA-CRISPR/Cas12a Assay. *Anal. chem.* **94**, 8277–8284 (2022).
28. Yin, K. et al. Dynamic aqueous multiphase reaction system for one-pot CRISPR-Cas12a-based ultrasensitive and quantitative molecular diagnosis. *Anal. chem.* **92**, 8561–8568 (2020).
29. Arizti-Sanz, J. et al. Streamlined inactivation, amplification, and Cas13-based detection of SARS-CoV-2. *Nat. commun.* **11**, 1–9 (2020).
30. Lu, S. et al. Fast and sensitive detection of SARS-CoV-2 RNA using suboptimal protospacer adjacent motifs for Cas12a. *Nat. Biomed. Eng.* **6**, 286–297 (2022).
31. Tong, X. et al. Fast and sensitive CRISPR detection by minimized interference of target amplification. *Nat. Chem. Biol.* **20**, 885–893 (2024).
32. Cheng, Z.-H. et al. Tunable control of Cas12 activity promotes universal and fast one-pot nucleic acid detection. *Nat. Commun.* **16**, 1166 (2025).

33. Hemphill, J., Borchardt, E. K., Brown, K., Asokan, A. & Deiters, A. Optical control of CRISPR/Cas9 gene editing. *J. Am. Chem. Soc.* **137**, 5642–5645 (2015).
34. Jain, P. K. et al. Development of light-activated CRISPR using guide RNAs with photocleavable protectors. *Angew. Chem. Int. Ed.* **55**, 12440–12444 (2016).
35. Nihongaki, Y., Kawano, F., Nakajima, T. & Sato, M. Photoactivatable CRISPR-Cas9 for optogenetic genome editing. *Nat. biotechnol.* **33**, 755–760 (2015).
36. Carlson-Stevermer, J. et al. CRISPRoff enables spatio-temporal control of CRISPR editing. *Nat. commun.* **11**, 5041 (2020).
37. Hu, M. et al. Photocontrolled crRNA activation enables robust CRISPR-Cas12a diagnostics. *P. Natl Acad. Sci. USA* **119**, e2202034119 (2022).
38. Chen, Y. et al. Photoactivatable CRISPR/Cas12a strategy for one-pot DETECTR molecular diagnosis. *Anal. Chem.* **94**, 9724–9731 (2022).
39. Hu M. et al. Light-start CRISPR–Cas12a reaction with caged crRNA enables rapid and sensitive nucleic acid detection. *Angew Chem. Int. Edit.* **62**, e202300663 (2023).
40. Liu P. et al. Universal crRNA Acylation Strategy for Robust Photo-Initiated One-Pot CRISPR–Cas12a Nucleic Acid Diagnostics. *Angew Chem. Int. Edit.* **63**, e202401486 (2024).
41. Zetsche, B. et al. Cpf1 is a single RNA-guided endonuclease of a class 2 CRISPR-Cas system. *Cell* **163**, 759–771 (2015).
42. Fonfara, I., Richter, H., Bratovič, M., Le Rhun, A. & Charpentier, E. The CRISPR-associated DNA-cleaving enzyme Cpf1 also processes precursor CRISPR RNA. *Nature* **532**, 517–521 (2016).
43. Yamano, T. et al. Crystal structure of Cpf1 in complex with guide RNA and target DNA. *Cell* **165**, 949–962 (2016).
44. Gao, P., Yang, H., Rajashankar, K. R., Huang, Z. & Patel, D. J. Type V CRISPR-Cas Cpf1 endonuclease employs a unique mechanism for crRNA-mediated target DNA recognition. *Cell res.* **26**, 901–913 (2016).
45. Mekler V. et al. CRISPR–Cas molecular beacons as tool for studies of assembly of CRISPR–Cas effector complexes and their interactions with DNA. In: Methods in enzymology). *Elsevier* (2019).
46. Lusic, H., Young, D. D., Lively, M. O. & Deiters, A. Photochemical DNA activation. *Org. Lett.* **9**, 1903–1906 (2007).
47. Shebanova, R. et al. Efficient target cleavage by Type V Cas12a effectors programmed with split CRISPR RNA. *Nucleic acids res* **50**, 1162–1173 (2022).
48. Korppi, M., Heiskanen-Kosma, T. & Kleemola, M. Incidence of community-acquired pneumonia in children caused by Mycoplasma pneumoniae: serological results of a prospective, population-based study in primary health care. *Respirology* **9**, 109–114 (2004).
49. Phillips, K., McCallum, N. & Welch, L. A comparison of methods for forensic DNA extraction: Chelex-100® and the QIAGEN DNA Investigator Kit (manual and automated). *Forensic Sci. Int-Gen.* **6**, 282–285 (2012).
50. Dong, D. et al. The crystal structure of Cpf1 in complex with CRISPR RNA. *Nature* **532**, 522–526 (2016).
51. Nguyen, L. T. et al. Harnessing noncanonical crRNAs to improve functionality of Cas12a orthologs. *Cell rep.* **43** (2024).
52. Swarts, D. C., van der Oost, J. & Jinek, M. Structural basis for guide RNA processing and seed-dependent DNA targeting by CRISPR-Cas12a. *Mo. cell* **66**, 221–233.e224 (2017).

Acknowledgements

This work was supported by National Key R&D Program of China 2023YFC2307400 (X.M.Z.), the Basic and Applied Basic Research Foundation of Guangdong Province 2021A1515220164 (X.M.Z.), 2023A1515220160 (M.C.), grants from the National Natural Science Foundation of China 32150019 (X.M.Z.), Guangdong Basic and Applied Basic Research Foundation Youth Fund project 2023A1515111076 (T.T.), China Postdoctoral Science Foundation 2023M741238 (T.T.).

Author contributions

X.M.Z. and T.T. conceived and designed the study. H.R.X. conducted the experiments. T.T. and H.R.X. contributed to the data analysis and interpretation. T.T. and X.M.Z. wrote the manuscript. M.C. collected and provided the clinical samples., T.Z., X.Y.G., W.W.Q., C.Y.X., M.Y.C., and P.G.C. assisted with sample processing and nucleic acid extraction. Z.Q.Q. designed and constructed the portable device. X.M.Z., T.T., and H.R.X. supervised the manuscript. All authors reviewed and approved the final manuscript.

Competing interests

All authors declare no competing interests.

Additional information

Supplementary information The online version contains supplementary material available at https://doi.org/10.1038/s41467-025-62082-5.

Correspondence and requests for materials should be addressed to Tian Tian or Xiaoming Zhou.

Peer review information *Nature Communications* thanks Changchun Liu, who co-reviewed with Jiongyu Zhang and the other, anonymous, reviewer for their contribution to the peer review of this work. A peer review file is available.

Reprints and permissions information is available at http://www.nature.com/reprints

Publisher's note Springer Nature remains neutral with regard to jurisdictional claims in published maps and institutional affiliations.

Open Access This article is licensed under a Creative Commons Attribution-NonCommercial-NoDerivatives 4.0 International License, which permits any non-commercial use, sharing, distribution and reproduction in any medium or format, as long as you give appropriate credit to the original author(s) and the source, provide a link to the Creative Commons licence, and indicate if you modified the licensed material. You do not have permission under this licence to share adapted material derived from this article or parts of it. The images or other third party material in this article are included in the article's Creative Commons licence, unless indicated otherwise in a credit line to the material. If material is not included in the article's Creative Commons licence and your intended use is not permitted by statutory regulation or exceeds the permitted use, you will need to obtain permission directly from the copyright holder. To view a copy of this licence, visit http://creativecommons.org/licenses/by-nc-nd/4.0/.

© The Author(s) 2025